INVERSE DESIGN OF TURBOMACHINERY AIRFOILS USING THE NAVIER-STOKES EQUATIONS

B. Kaplan and S. Eyi
Aeronautical Engineering
Middle East Technical University
Ankara, 06531 Turkey

Abstract

In this paper an inverse design method is presented which couples a Navier-Stokes flow solver and a numerical optimization algorithm. The design method generates a turbomachinery airfoil, producing a specified surface pressure distribution at a transonic speed. A least-square optimization technique is used to minimize pressure discrepancies between the target and designed airfoils. In order to represent the non-linear, rotational and viscous physics of transonic flows, Navier-Stokes equations are used to predict the flow field. Sensitivity derivatives are obtained using finite differencing. Effects of different design variables on the performance of design optimization are evaluated.

1 Introduction

Computational fluid dynamics (CFD) has changed the aerodynamic design process. CFD was first employed in design in a cut-and-try manner by utilizing its flow analysis capability. That is, a specified configuration is first evaluated to get its aerodynamic performance characteristics, and then the geometry is modified to produce an improved performance. While this methodology may be effective if the designs fall within a known experimental database, it becomes cumbersome and difficult when the design progresses outside the domain of the known database. This type of design methods for turbomachinery system was discussed in Reference 1. Clearly, more automated design optimization technologies are desirable for the development of new turbomachinery components. As computational methods have advanced, CFD-based numerical optimization became a more viable design tool for advanced turbomachinery components.

A unique advantage of CFD is the capability of inverse design. Inverse design finds the airfoil geometry that produces the pressure or velocity distributions specified by a designer. Earlier inverse design methods were based on the potential equation due to its simplicity. [2,3] The potential formulation, however, can not properly represent the transonic features such as embedded shock waves and shock-boundary-layer interactions. Several inverse design methods were demonstrated using the Euler equations. [4,5] In order to improve the reliability of a design, viscous effects were often incorporated by using the boundary-layer equations. However, the Euler and boundary-layer coupling fails when the flow separates. Hence even a temporary occurrence of separation can terminate the design process. Therefore, several recent inverse design methods used the Navier-Stokes equations. [6]

Inverse design based on the Euler and Navier-Stokes equations has a difficulty in formulating the inverse problem. Therefore, an iterative approach is often incorporated to improve the guess of the target airfoil starting from a known geometry. Some inverse designs use stochastic methods such as genetic algorithms. [7] Stochastic methods have more advantages in finding globally optimum solution. However, these methods require large number of function evaluations and may not be suitable for practical design applications. In the present study, a deterministic method based on a least-square optimization is used. In the

following sections, the technology pieces used are first described and then results from design practices are presented.

2 Flow Analysis

The two-dimensional, unsteady, compressible Navier-Stokes equations are solved using a body-fitted, curvilinear co-ordinate system. The Baldwin-Lomax eddy viscosity model [8] is used for turbulence closure, and the transition point is fixed at fourteen percent of the chord. A finite volume method is employed for the spatial discretization. The flow variables are defined at cell centers, and centered differencing is used for the spatial derivatives. Second- and fourth-order artificial viscosities are added to enforce numerical stability. [9,10] The time integration is performed using an explicit, four-stage Runge-Kutta scheme. Local time stepping, variable-coefficient implicit residual smoothing, and a multigrid method are implemented to accelerate the convergence. Characteristic boundary conditions are imposed at the far-field boundary based on a one-dimensional eigenvalue analysis, and a no-slip, adiabatic-wall conditions are used on the airfoil surface.

3 Numerical Optimization

The design process starts with a guess for the target airfoil geometry, namely an initial baseline airfoil. The flow analysis of the baseline airfoil examines the quality of the guess in producing the specified target pressure. Using an initial airfoil with its pressure distribution already close to the target pressure would speed up the design process. The airfoil geometry is updated by adding a smooth perturbation. The geometry perturbation normal to camber-line, Δy, is defined as a linear combination of the shape functions, f_k:

$$\Delta y(x) = \sum_{k=1}^{K} \delta_k f_k(x) \qquad (1)$$

where x is the normalized position of the camber-line, y is the axis perpendicular to camber-line, and K stands for the number of the shape functions. The weighting coefficients, δ_k, in the equation are the design variables to be determined through an optimization process. Figure 2 shows a schematic of the optimization procedure.

In order to judge the design quality and monitor the convergence of the design cycle, a convergence parameter, CP, is defined. This parameter is based on the root-mean-square of length-weighted pressure discrepancies between the target pressure and the pressure of the designed airfoil:

$$CP = \left(\frac{\sum_{i=1}^{I} \left(P_{t_i} - P_{b_i} \right)^2 \Delta S_i}{\sum_{i=1}^{I} \Delta S_i} \right)^{\frac{1}{2}} \qquad (2)$$

where P_{t_i} and P_{b_i} are the target and baseline pressures respectively on the airfoil surface at point i and ΔS_i is the length of the surface element. There are a total of I elements on the airfoil.

The objective function to be minimized is chosen as follows:

$$J = \sum_{i=1}^{I} \left(P_{t_i} - P_{b_i} - \sum_{k=1}^{K} \frac{\partial P_i}{\partial \delta_k} \delta_k \right)^2 \Delta S_i \qquad (3)$$

where $\partial P_i / \partial \delta_k$ is the response of the flow field due to a small perturbation and is estimated using a finite difference:

$$\frac{\partial P_i}{\partial \delta_k} = \frac{P_i(y + \delta f_k) - P_i(y)}{\delta} \qquad (4)$$

for a small value of δ. The same Navier-Stokes code is used to evaluate the change in the surface pressure due to a small geometry perturbation defined by each shape function.

Then the magnitude of each perturbation, δ_k, needed to achieve the target pressure distribution is determined by a least-square optimization technique. That is, the minimization condition yields

$$\frac{\partial J}{\partial \delta_j} = 0 = -2\sum_{i=1}^{I}\left(P_{t_i} - P_{b_i} - \sum_{k=1}^{K}\frac{\partial P_i}{\partial \delta_k}\delta_k \right)\frac{\partial P_i}{\partial \delta_j}\Delta S_i \quad (5)$$

for j=1,K. It can be rewritten as

$$\sum_{k=1}^{K}\left(\sum_{i=1}^{I}\frac{\partial P_i}{\partial \delta_j}\frac{\partial P_i}{\partial \delta_k}\Delta S_i \right)\delta_k = \sum_{i=1}^{I}\frac{\partial P_i}{\partial \delta_j}\left(P_{t_i} - P_{b_i} \right)\Delta S_i \quad (6)$$

for j=1,K. Equation (6) is solved for the δ_k's that define the perturbation, Δy, required to improve the guess. This procedure is repeated iteratively.

4 Design Variables

In general, turbomachinery airfoil design involves different disciplines such as fluid mechanics, heat transfer, materials, acoustics, etc. Therefore, all significant physics should be considered in selecting design variables and constraints. However, increasing the number of design constraints and/or variables will increase the design cost. An appropriate choice of design variables may reduce the number of design constraints required while increasing design performance.

The performance of a design process is strongly influenced by the choice of shape functions because shape functions influence the convergence rate of the optimization process as well as the quality of design results. The present study examines the following three different shape functions shown in Figure 3.

Wagner Functions:

The Wagner functions provide large variations with high harmonics and may cause waviness in resulting designs.

$$f_1(x) = \frac{[\theta + \sin(\theta)]}{\pi} - \sin^2\left(\frac{\theta}{2}\right) \quad (7)$$

$$f_k(x) = \frac{\sin(k\theta)}{k\pi} + \frac{\sin[(k-1)\theta]}{\pi} \text{ for } k > 1$$

where

$$\theta = 2\sin^{-1}\left(\sqrt{x}\right)$$

Patched Polynomials:

A cubic on one side of x_k is patched with another cubic on the other side to produce a smooth curve of second-order continuity. x_k is the location of maximum perturbation.

$$f_k(x) = 1 - \left(\frac{x - x_k}{x_k}\right)^2\left(1 + \frac{A}{(1-x_k)^2}\frac{x}{x_k}\right)$$

for $0 \le x \le x_k$ (8)

$$f_k(x) = 1 - \left(\frac{x - x_k}{1 - x_k}\right)^2\left(1 + \frac{B}{(x_k)^2}\frac{1-x}{1-x_k}\right)$$

for $x_k \le x \le 1$

where

$$A = \max(0, 1 - 2x_k)$$

$$B = \max(0, 2x_k - 1)$$

x_k = 0.05, 0.1, 0.2, 0.3, 0.5, 0.7, 0.8, 0.9 ,0.95

Hicks-Henne Functions:

The sinusoidal shape functions are frequently used in airfoil optimization.

$$f_k(x) = \sin^3\left(\pi x^{e(k)}\right) \quad (9)$$

where

$$e(k) = \frac{\log(0.5)}{\log(x_k)}$$

x_k = 0.05, 0.1, 0.2, 0.3, 0.5, 0.7, 0.8, 0.9 ,0.95

Here x_k's are the locations of maximum height of corresponding shape functions.

5 Results

The goal of the present study is to evaluate the performance, dependency, consistency, and cost of the present inverse design method. Effects of different types of shape functions on the design performance are evaluated with the given turbomachinery airfoil. All the design practices are performed using a C-type grid and the size of 257×49. The minimum grid spacing next to

the airfoil surface is set to .001 percent of the chord length. Figure 1 shows the fine grid used in this study. Flow calculations are started with the most recent solutions and terminated when the maximum residuals are reduced five orders of magnitude with respect to the free-stream initial solution.

The design practices are performed for the Rotor R 030. [11] The profiles at 170 and 190 mm. in radial axis are used as target and baseline airfoils, respectively. The flow condition is set to $M_2 = 0.8$, $M_1 = 1.25$, $\alpha = 60°$ and $Re = 10^6$. Here, M_2 , M_1, α and Re are the outlet and inlet Mach numbers, inlet flow angle and Reynolds number, respectively.

In this study, Wagner functions, Patched polynomials and Hicks-Henne functions modify the upper and lower surface of the airfoil. A total of sixteen and eighteen shape functions are used. Effects of different perturbation sizes on the convergence of designs are evaluated. Figures 4 to 9 show comparison of surface pressure and airfoil geometries between initial, target and designed airfoils. Convergence histories are also compared for different perturbation sizes. For the designed airfoil, only results with the best convergence are shown.

In designs with Wagner functions and Patched polynomials, increasing the number of shape functions from sixteen to eighteen does not improve the design convergence significantly. However, increasing the number of shape functions shows significant improvements in design with Hicks-Henne functions. The best convergence is achieved with 16 Wagner functions. Better convergence may be achieved by changing the location of the maximums of Hicks-Henne functions and Patched polynomials.

In most of the design practices, the converged results are obtained within five design cycles. The convergence of design is influenced by perturbation size. The finite difference evaluation of the sensitivity may introduce two different errors: truncation error and condition error. The truncation error is the result of neglected terms in the Taylor series expansion and decreases with the decreasing perturbation size. The condition error comes from an early termination of the iteration in a flow solution process. In most of the design practices, the best convergence is achieved with a perturbation size of .00075 and .00100.

Tables 1 and 2 show the convergence parameter and CPU time after ten design cycles. All designs are performed on an eight processor IBM SP2. The design with 18 Hicks-Henne functions takes the minimum CPU time. Some design practices take large CPU time because it is difficult to have converged flow solution around the geometries obtained during the design cycles.

6 Concluding Remarks

The present paper demonstrates an inverse design method based on the Navier-Stokes equations for turbomachinery design. The use of Navier-Stokes equations improves the level of confidence on the design result. The performance of the design procedure is a function of the number and type of shape functions and the perturbation size used in the finite difference sensitivity evaluation. The present design method can be easily incorporated with the parallel computer architecture by assigning the sensitivity evaluation for each shape function to different processors.

References

[1] Jennions, I K. *Elements of Modern Turbomachinery Design System*. AGARD-LS-195, May 1994.

[2] Sanz, J M. Design of Supercritical Cascades with High Solidity. *AIAA Journal*, Vol. 21, No. 9, pp.1289-1293, September 1983.

[3] Dulikravich G S and Sobieczky H. Shockless Design and Analysis of Transonic Shapes. *AIAA Journal*, Vol. 20, No. 11, pp. 1572-1587, November 1982.

[4] Demeulenaere A , Leonard O and Van Den Braembussche R. Application of a Three-Dimensional Inverse Method to the Design of a Centrifugal Compressor Impeller. *Int. Gas Turbine & Aeroengine Congress & Exhibition*, Stockholm, Sweden, ASME Paper 98-GT-127, June 1998.

[5] Borges J E, Gato L M C and Pereira R M R J. Iterative Use of a Time-Marching Code for Designing Turbomachine Blade Rows. *Computers & Fluids*, Vol. 25, No. 2, pp. 197-216, 1996.

[6] Rai M M and Madavan N K. Application of Artificial Neural Networks to the Design of Turbomachinery Airfoils. *36th Aerospace Sciences Meeting & Exhibit*, Reno, NV, AIAA Paper 98-1003, January 1998.

[7] Vicini A and Quagliarella D. Inverse and Direct Airfoil Design Using a Multiobjective Genetic Algorithm. *AIAA Journal*, Vol. 35, No. 9, September 1997.

[8] Baldwin B S and Lomax H. Thin Layer Approximation and Algebraic Model for Separated Turbulent Flows. *AIAA 16th Aerospace Sciences Meeting*, Huntsville, AL, AIAA 78-0257, January 1978.

[9] Martinelli L, Jameson A and Grasso F. A Multigrid Method for the Navier Stokes Equations. AIAA Paper 86-0208, 1986.

[10] Arnone A and Swanson R C. A Navier-Stokes Solver for Cascade Flows. NASA-CR-181682, 1988.

[11] Dunker R. Test Case E/CO-4: Single Transonic Compressor Stage. *AGARD Advisory Report No:275*, pp. 245-285, 1990.

Table 1. Design with 16 shape functions:

(a) With Wagner functions

Delta	Convergence	CPU(hrs)
.00150	.00302569	45.21
.00125	.00275943	49.77
.00100	.00279145	70.92
.00075	.00277741	61.76
.00050	.00287570	60.64

(b) With Patched polynomials

Delta	Convergence	CPU(hrs)
.00150	.00377246	49.51
.00125	.00376381	55.20
.00100	.00383265	46.26
.00075	.00374078	42.37
.00050	.00378255	42.28

(c) With Hicks-Henne functions

Delta	Convergence	CPU(hrs)
.00150	.01724246	45.91
.00125	.01705344	38.95
.00100	.00886708	32.75
.00075	.00912446	51.16
.00050	.00886751	29.00

Table 2. Design with 18 shape functions:

(a) With Wagner functions

Delta	Convergence	CPU(hrs)
.00150	.00381642	64.66
.00125	.00309379	64.21
.00100	.00334132	69.21
.00075	.00307856	70.15
.00050	.00344490	57.09

(b) With Patched polynomials

Delta	Convergence	CPU(hrs)
.00150	.00388536	49.50
.00125	.00358294	50.80
.00100	.00408703	42.72
.00075	.00362037	39.04
.00050	.00357356	47.50

(c) With Hicks-Henne functions

Delta	Convergence	CPU(hrs)
.00150	.00337121	34.88
.00125	.00349952	38.97
.00100	.00345400	38.01
.00075	.00339138	39.14
.00050	.00333313	23.33

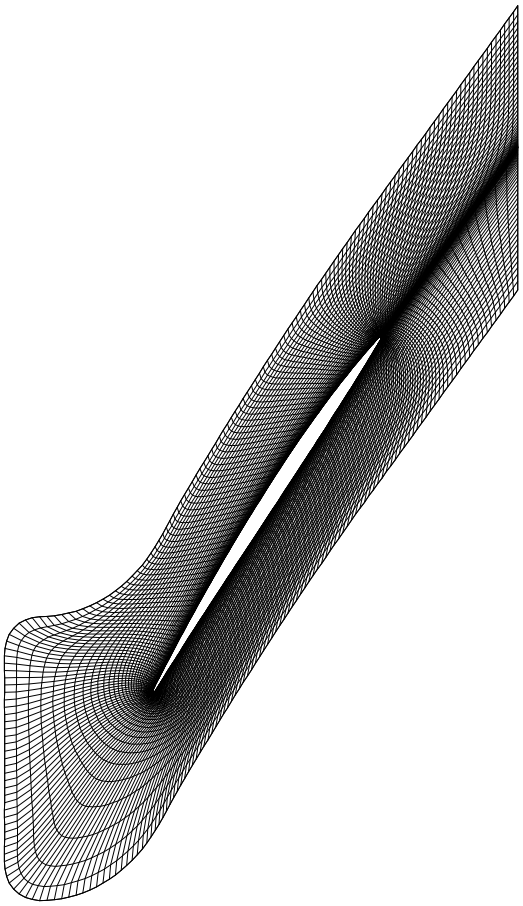

Figure 1. Computational grid (257x49)

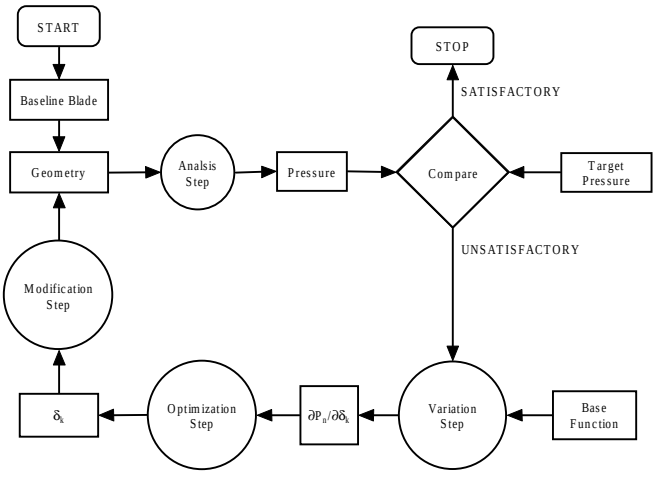

Figure 2. Design optimization procedure

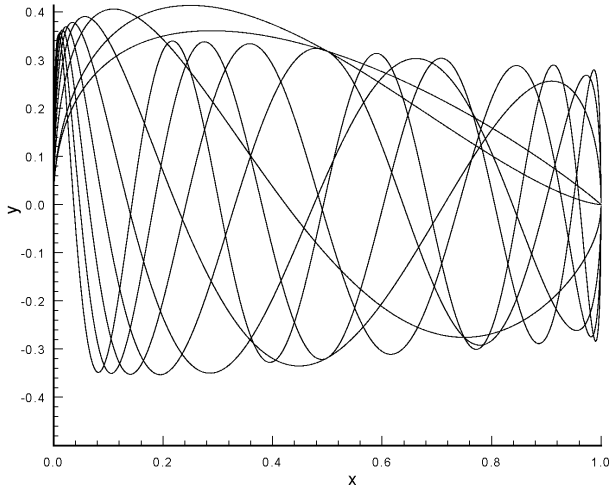

(a) Wagner functions

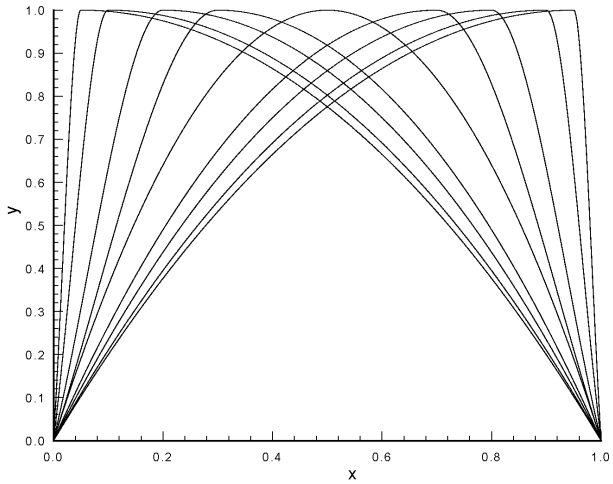

(b) Patched polynomials

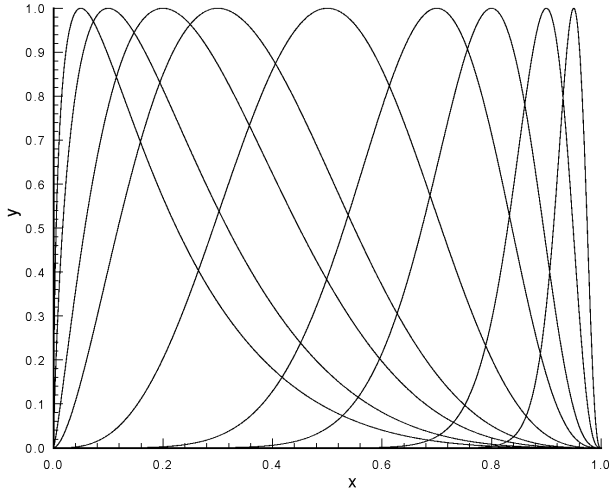

(c) Hicks-Henne functions

Figure 3. Shape functions used to perturb the geometry

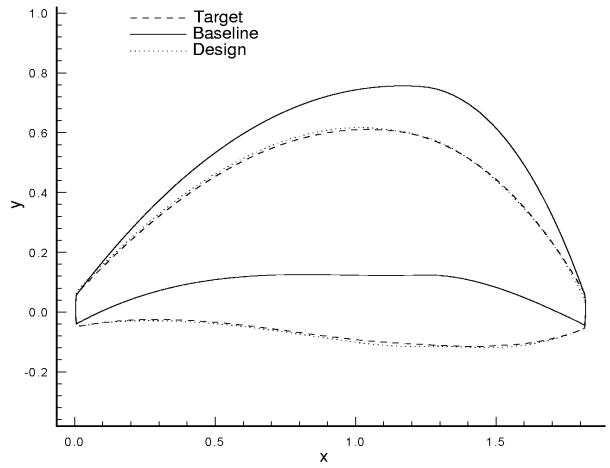

(a) Evolution of blade geometry

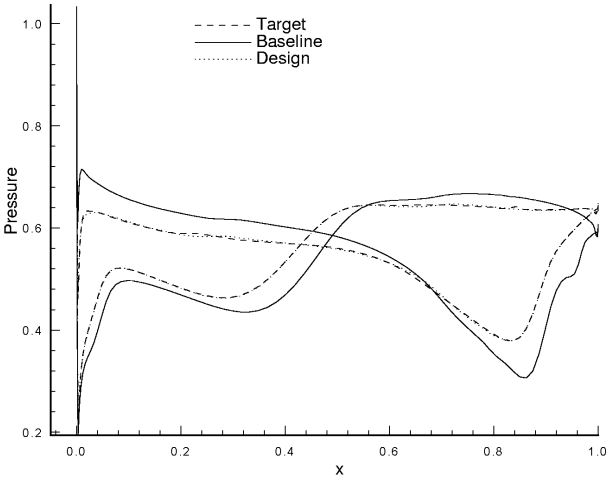

(b) Evolution of surface pressure

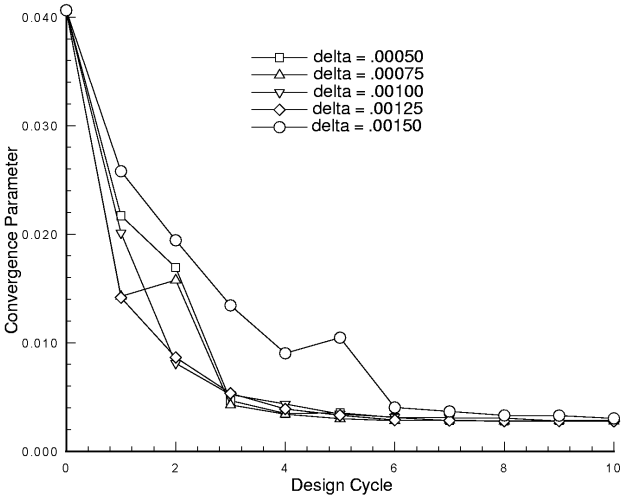

(c) Convergence history

Figure 4. Design practice with 16 Wagner functions

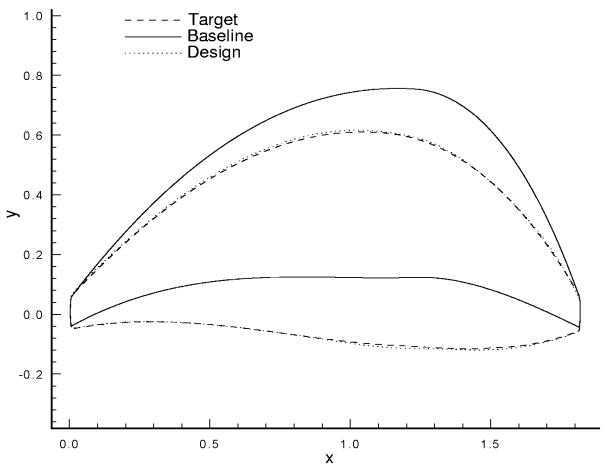

(a) Evolution of blade geometry

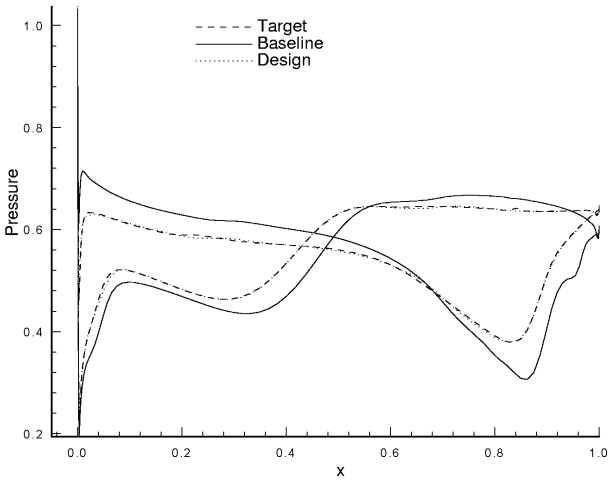

(b) Evolution of surface pressure

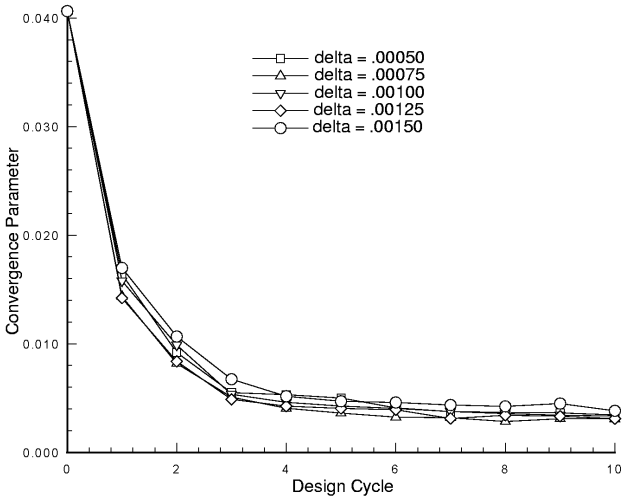

(c) Convergence history

Figure 5. Design practice with 18 Wagner functions

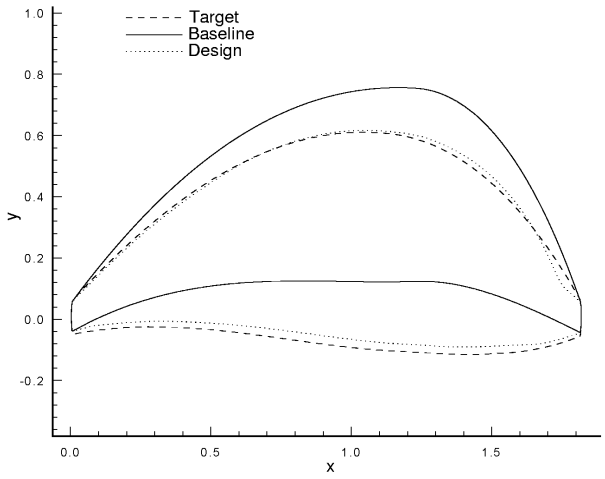

(a) Evolution of blade geometry

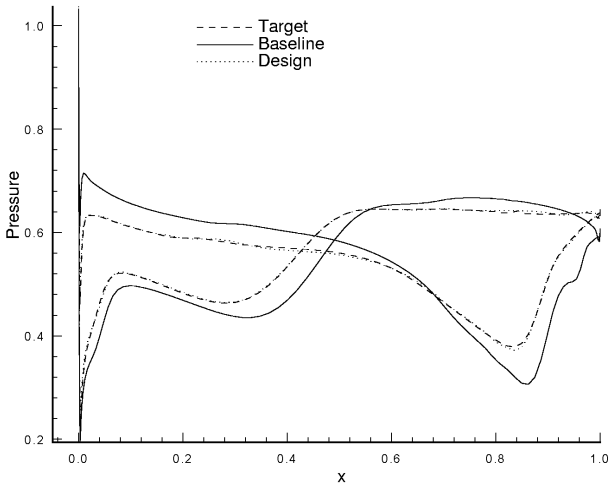

(b) Evolution of surface pressure

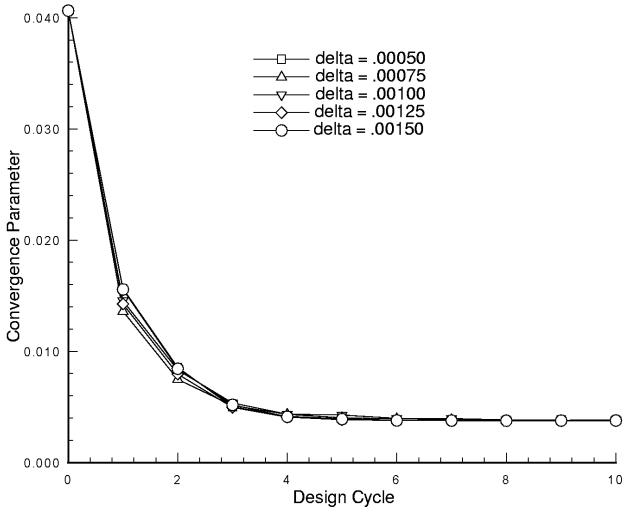

(c) Convergence history

Figure 6. Design practice with 16 Patched polynomials

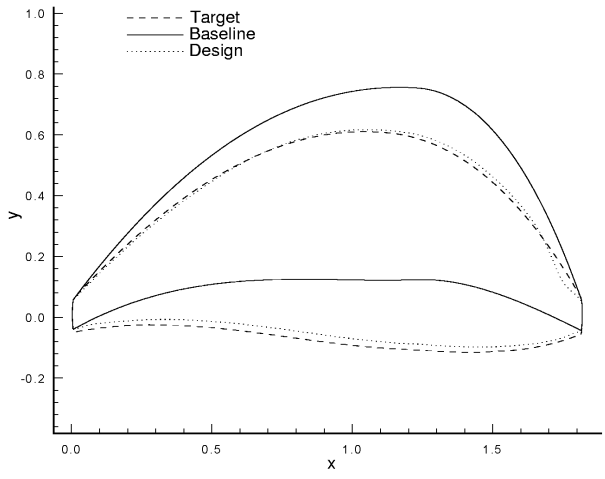

(a) Evolution of blade geometry

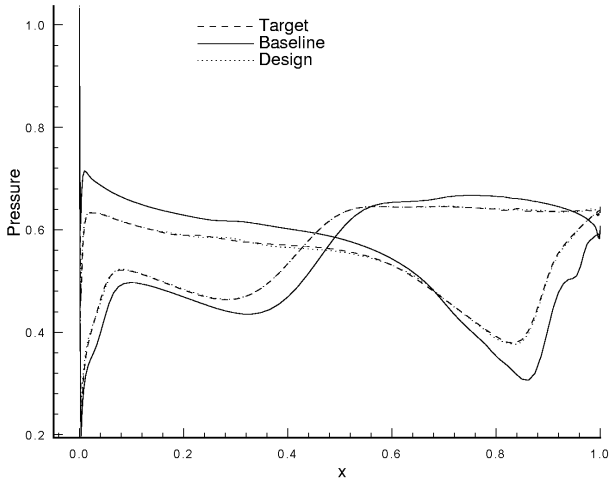

(b) Evolution of surface pressure

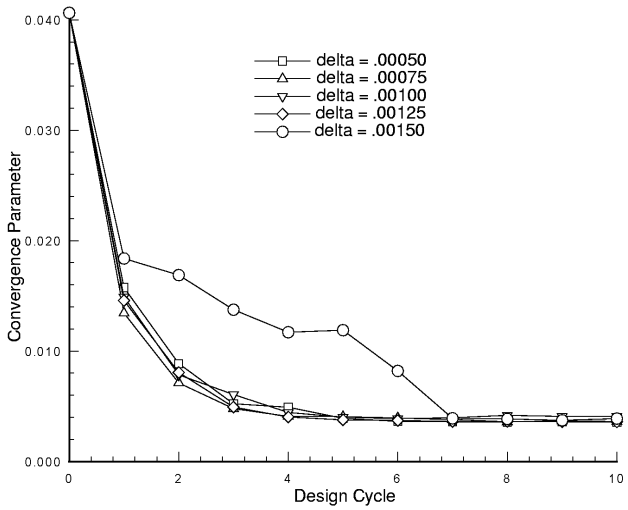

(c) Convergence history

Figure 7. Design practice with 18 Patched polynomials

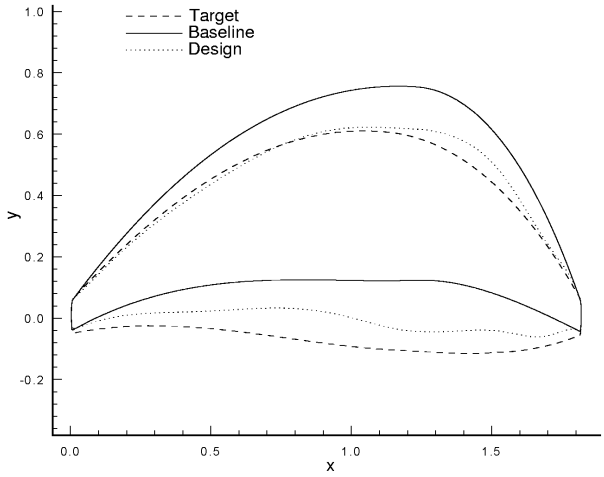

(a) Evolution of blade geometry

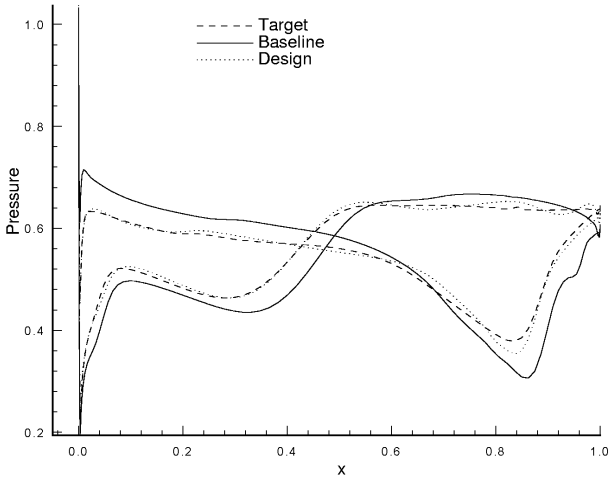

(b) Evolution of surface pressure

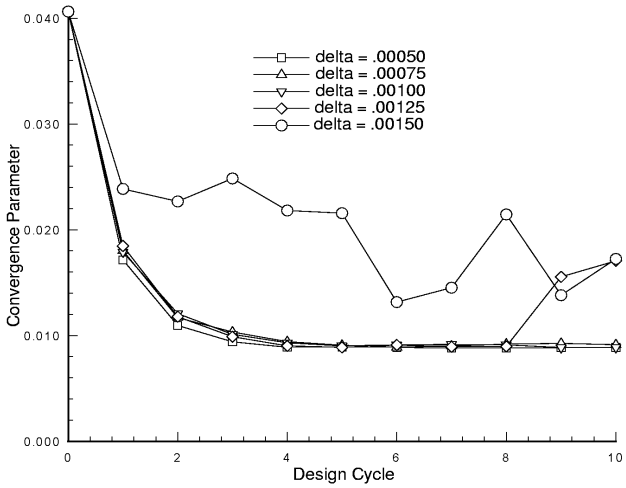

(c) Convergence history

Figure 8. Design practice with 16 Hicks-Henne functions

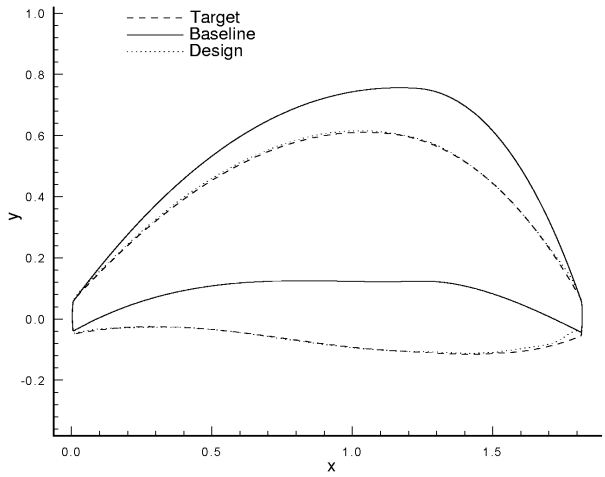

(a) Evolution of blade geometry

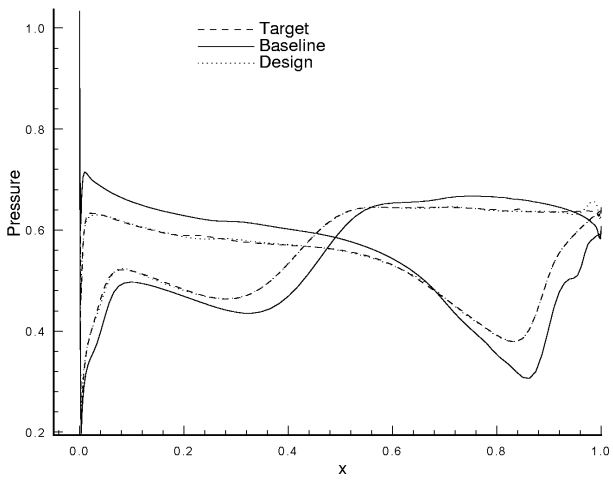

(b) Evolution of surface pressure

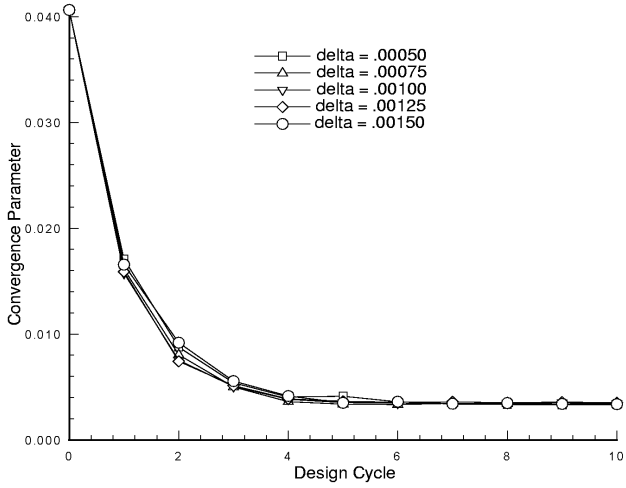

(c) Convergence history

Figure 9. Design practice with 18 Hicks-Henne functions